Microscopic study of nuclear structure for some Si-isotopes using Skyrme-Hartree-Fock-method

Zaheda.A.Dakhil[1], Ali A. Alzubadi[1], Sheimaa T. Aluboodi[2]

[1]Department of Physics, College of Science, University of Baghdad

[2]Dijlah College University- Baghdad-Iraq

E-mail: sheimaathiab@yahoo.com

Abstract

In this paper the nuclear structure of some of Si-isotopes namely, ^{28,32,36,40}Si have been studied by calculating the static ground state properties of these isotopes such as charge, proton, neutron and mass densities together with their associated rms radii, neutron skin thicknesses, binding energies, and charge form factors. In performing these investigations, the Skyrme-Hartree-Fock method has been used with different parameterizations; SkM*, S1, S3, SkM, and SkX. The effects of these different parameterizations on the above mentioned properties of the selected isotopes have also been studied so as to specify which of these parameterizations achieves the best agreement between calculated and experimental data. It can be deduced from this study that it is SkX parameterization that achieves such agreement. Furthermore, comparison between the theoretical and experimental results of charge form factors has been performed.

دراسة مجهرية للتركيب النووي لبعض نظائر نواة السليكون باستخدام طريقة سكيرم-هارتري-فوك

زاهدة احمد دخيل[1]، علي عبد اللطيف[1]، شيماء ذياب عطية[2]

[1]قسم الفيزياء، كلية العلوم، جامعة بغداد

[2]كلية دجلة الجامعة

الخلاصة

يتناول هذا البحث دراسة التركيب النووي لبعض نظائر السيليكون ^{28,32,36,40}Si من خلال حساب خواص الحالة الارضية لها مثل كثافة كل من الشحنة، البروتون، النيوترون والكتلة مع انصاف الاقطار المرافقة لها و كذلك حساب السمك النيوتروني وطاقات الربط وعوامل تشكل الشحنة. تم استخدام طريقة سكيرم هارتري فوك في تنفيذ هذه الدراسة مع باراميترات مختلفة وهي SkM* و S1 وS3 وSkM وSkX. لقد تمت دراسة تاثير هذه البارامترات المختلفة على خواص النظائر المذكورة اعلاه وذلك لتحديد اي من هذه البارامترات يحقق افضل تطابق مع الحسابات العملية لتلك الخواص. ويستنتج من هذه الدراسة ان SkX يتفوق على بقية البارامترات في تحقيق هذا التطابق. كما تمت المقارنة بين النتائج النظرية والتجريبية لعوامل تشكل الشحنة.

Introduction

In studying the nuclear structure, the development of the proposed nuclear models is determined by the experimental observations of the nuclei behavior. The Skyrme effective interaction was first proposed in late 1950 [1]. By the work of Vautherin and Brink, the Skyrme interaction was introduced in the Hartree-Fock (HF) calculations of nuclei [2]. Until now, the Skyrme-Hartree-Fock (SHF) method has been

successfully and widely used for studying the nuclear structure [3].

The nuclear charge density distribution is one of the basic quantities for describing the nuclear structure. It can give detailed information on the internal structure of nuclei since they are directly related to the wave functions of the protons which are important keys to many calculations in nuclear physics. Also the nuclear charge radii represent the most useful observables for analyzing the nuclear structure. These observables provide information about the nuclear shape which can be determined from the form factors.

The ground state properties of ^{28,32,36,40}Si isotopes will be investigated in details using the SHF method for calculating charge, proton, neutron and mass densities, and the rms radii of charge distributions, neutron skin thicknesses, binding energies, and form factors. The calculated results will then be compared with the experimental data available for the said isotopes.

Theory

The Skyrme force is an effective interaction with a two-body and three-body parts [4]. The two-body term is written as a short-range expansion with the form [5]:

$$V = \sum_{i<j} V_{ij}^{(2)} + \sum_{i<j<k} V_{ijk}^{(3)}, \tag{1}$$

where:

$$V_{Skyrme} = \sum_{i<j} V_{ij}$$

$$V_{Skyrme} = t_0\left(1 + x_0 \hat{P}_\sigma\right)\delta(\vec{r}) + \frac{1}{2}t_1\left(1 + x_1 \hat{P}_\sigma\right)\left[\delta(\vec{r})\vec{k}^2 + \vec{k}'^2\delta(\vec{r})\right]$$
$$+ t_2\left(1 + x_2 \hat{P}_\sigma\right)\vec{k}'.\delta(\vec{r})\vec{k} + \frac{1}{6}t_3\left(1 + x_3 \hat{P}_\sigma\right)\rho^\alpha(\vec{R})\delta(\vec{r})$$
$$+ it_4\vec{k}'.\delta(\vec{r})(\vec{\sigma}_i + \vec{\sigma}_j)\vec{k} \tag{2}$$

where the $\hat{k}$ and $\hat{k}'$ operators are the relative (momentum) wave vectors of two nucleons. $\hat{k}$ acts to the right and $\hat{k}'$ to the left. They have the form:

$$\hat{k} = \frac{1}{2i}(\nabla_1 - \nabla_2) \Rightarrow \hat{k}^2 = -\frac{1}{4}(\nabla_1^2 - \nabla_2^2 - 2\nabla_1 \cdot \nabla_2)$$
$$\hat{k}' = -\frac{1}{2i}(\nabla_1' - \nabla_2') \Rightarrow \hat{k}'^2 = -\frac{1}{4}(\nabla_1'^2 - \nabla_2'^2 - 2\nabla_1' \cdot \nabla_2')$$

$\delta(\vec{r})$ is the delta function. $\hat{P}_\sigma$ is the space exchange operator, $\vec{\sigma}$ the vector of Pauli spin matrices and the $t_0, t_1, t_2, t_3, t_4, x_0, x_1, x_2, x_3$ and α are the Skyrme force parameters describing the strengths of the different interaction terms[6]. The values of these parameters for different Skyrme parameterizations: SkM* [7], S1, S3 [2], SkM [8], and SkX [9] are listed in Table1.

The Hamiltonian is written in terms of kinetic energy and two-body nucleon-nucleon interaction [10]:

$$\hat{H} = \sum_{i=1}^{A} \frac{\hat{p}_i^2}{2m_i} + \frac{1}{2}\sum_{i \neq j}^{A} V(r_i, r_j). \tag{3}$$

In this representation of Hamiltonian the nucleon-nucleon interaction characterizes the many-particle Schrödinger equation. In the SHF approach the total binding energy of the

system is given by the sum of the kinetic and Coulomb energies as well as the Skyrme

energy functional that models the effective interaction between nucleons[11]

$$E = E_{Coul} + E_{Kin} + \int \varepsilon_{Sky} dr + E_{pair} + E_{Cm}. \tag{4}$$

Table 1: The values of Skyrme parameterizations.

Force	SkM*	S1	S3	SkM	SkX
t0 (MeV· fm3)	−2645.0	−1057.3	−1128.75	−2645.0	-1445.3
t1 (MeV· fm5)	410	235.9	395	385	246.9
t2 (MeV · fm5)	−135.0	−100.0	−95.0	−120.0	-131.8
t3 (MeV · fm3)	15595	14463.5	14000	15595	12103.9
t4 (MeV · fm5)	130	0	120	130	
x0	0.09	0.56	0.45	0.09	0.34
x1	0	0	0	0	0.58
x2	0	0	0	0	0.127
x3	0	1	1	0	0.03
α	1/6	1	1	1/6	0.5

The expectation value of the HF Hamiltonian or energy of the system can be re-written as a spatial integral over a Hamiltonian density:

$$E = \int d^3 r \hat{H}(r) \tag{5}$$

By substituting the Skyrme interaction terms into the full energy expression, the form of the density function $\hat{H}(r)$ can be written as [12].

$$\langle \Phi | \hat{H} | \Phi \rangle = -\frac{\hbar^2}{2m} \sum_{i=1}^{A} \int dr_1 \, \emptyset_i^*(r_1) \nabla_i^2 \emptyset_i(r_1)$$

$$+\frac{1}{2} \sum_{ij\sigma_1\sigma_2 q_1 q_2} \iint d^3r_1 d^3r_2 \phi_i^*(r_1, \sigma_1, q_1) \phi_j^*(r_2, \sigma_2, q_2)$$

$$V(r_1, r_2)\left(1 - \hat{P}_M \hat{P}_\sigma \hat{P}_q\right) \phi_i(r_1, \sigma_1, q_1) \phi_j(r_2, \sigma_2, q_2). \tag{6}$$

The present research is primarily concerned with the properties of the ground-state charge density $\rho(r)_{ch}$, which gives the most direct

physical insight into the distribution of protons inside the nucleus. The densities $\rho(r)$ in spherical representation are given by [13]:

$$\rho_q(r) = \sum_{n_\beta j_\beta l_\beta} \omega_\beta \frac{2j_\beta + 1}{4\pi} \left(\frac{R_\beta}{r}\right)^2, \tag{7}$$

where q represents the neutron, proton and charge, ω_β is occupation probability of the state β and j_β is the current density that vanishes for ground states. The charge probability density [13]:

$$P(r)_{ch} = 4\pi r^2 \rho(r)_{ch} \tag{8}$$

$P(r)_{ch}$ represents the probability to find Z protons at a given radius r from the center of the nucleus. The rms radii of neutron, proton, charge and mass distributions can be evaluated from these densities [14] as:

$$r_q = \langle r_q^2 \rangle^{1/2} = \left[\frac{\int r^2 \rho_q(r) dr}{\int \rho_q(r) dr}\right]^{1/2} \tag{9}$$

A quantity of both theoretical and experimental interest, the neutron skin thickness **t**, can then be defined as the difference between the neutron rms radius and the proton rms radius [15]:

$$t = r_n - r_p = \langle r_n^2 \rangle^{1/2} - \langle r_p^2 \rangle^{1/2}. \quad (10)$$

The concept of form factor is associated with the charge density and its properties. Elastic electron scattering from nuclei constitutes an important source of experimental data on charge densities which are measurable and with which the models for nuclear ground states can be tested. Electron scattering evolved from the early determinations of rms charge radii to the present much more precise measurements that have led to almost model- independent determinations of the charge density distributions of many nuclei. In these density distributions one can observe oscillations in the interior density which oscillations represent quantum "waves" in the nucleus [16]. Denoting by $F(q)$ the ratio of the electron scattering cross section to the Rutherford cross section (scattering from a point) as a function of momentum transfer, q, one can find that this ratio expresses the plane-wave Fourier transform of the charge density as follows[17]:

$$F(q) = \frac{1}{z} \int \rho(r)_{ch} e^{i\vec{q}.\vec{r}} \, d\tau = \frac{4\pi}{z} \int \rho(r)_{ch} j_0(qr) r^2 dr, \quad (11)$$

where the spherical Bessel function is:

$$j_0(qr) = \frac{\sin qr}{qr} \quad (12)$$

The normalization in Eq. (11) is chosen to give $F(q = 0)$ =1. For light nuclei the electron energy distortion is small, and the cross section is closely proportional to the form factor $|F(q)|^2$ which has minima corresponding to the zero of the function $F(q)$. For heavy nuclei the electron energy distortion is larger and the minima in the cross sections disappear. From an analysis of the electron scattering cross section the ratio $F(q)$ can be extracted with good precision over the range of momentum transfers measured. Consequently, from the measured form factors $|F(q)|^2$ the charge density can be obtained with the inverse of Eq. (11) [16]:

$$\int \rho(r)_{ch} dr = \frac{z}{2\pi^2} \int F(q) j_0(qr) q^2 dq \quad (13)$$

Results and discussions

For the sake of comparison the charge, proton, neutron and mass densities of the ^{28,32,36,40}Si isotopes are calculated by the five Skyrme parameterizations stated previously and drawn in Figs. 1and 2.
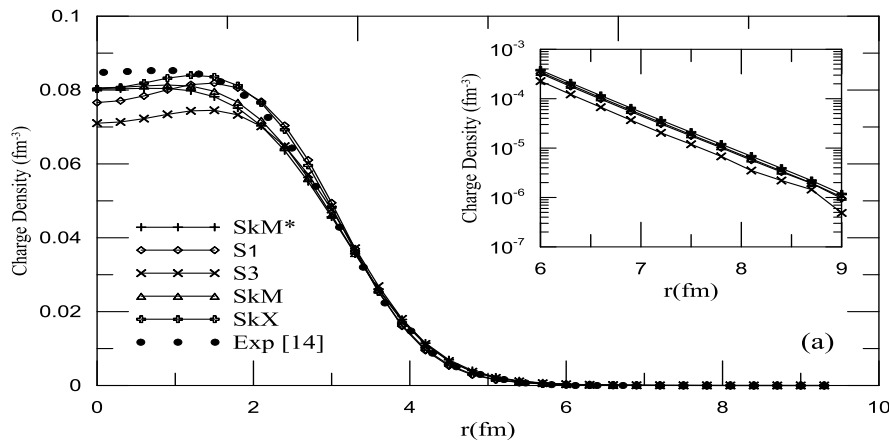

Fig. 1: Density curves of ^{28}Si as functions of radii calculated by different Skyrme parameterizations; (a) charge density
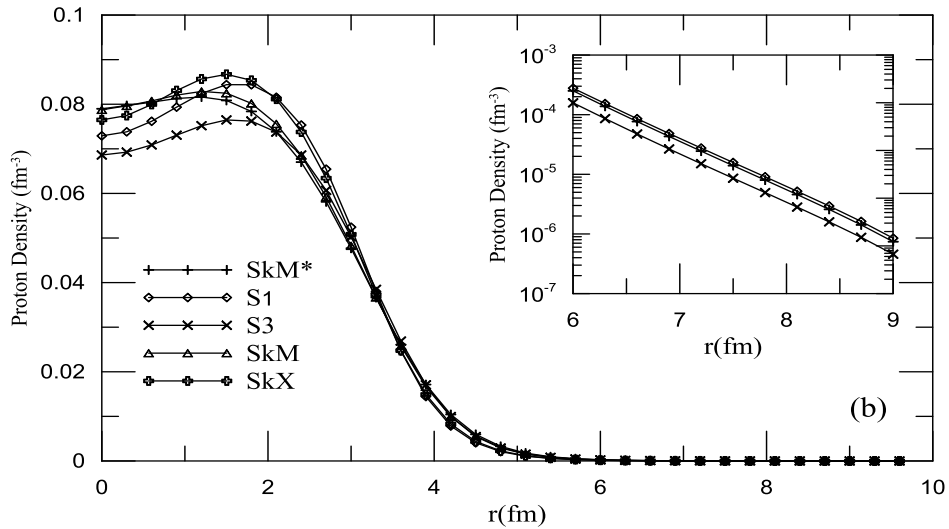
Fig. 1: Density curves of ^{28}Si as functions of radii calculated by different Skyrme parameterizations; (b) proton density.
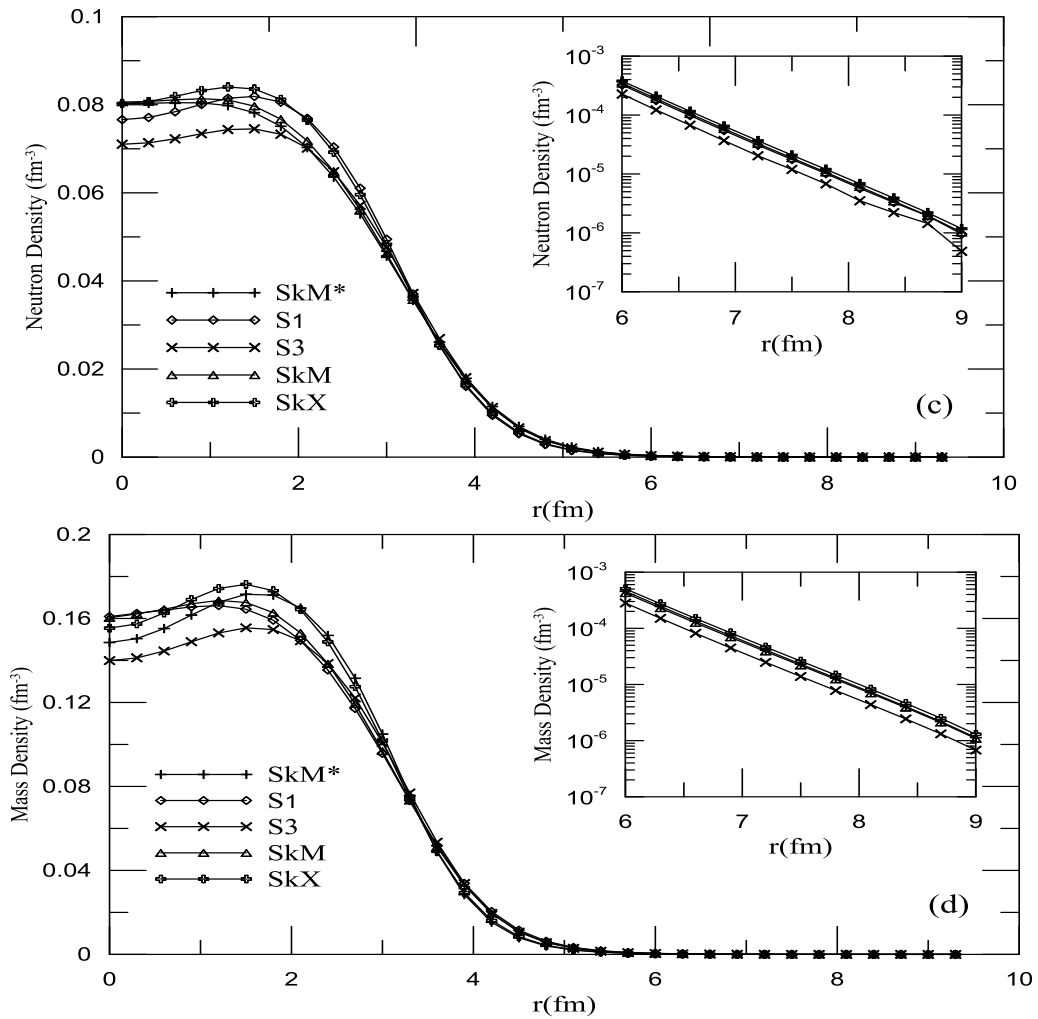

Fig.2: Density curves of ^{28}Si as functions of radii calculated by different Skyrme parameterizations; (c) neutron density, (d) mass density.

It can be seen clearly from the above density profiles that the best agreement between the experimental data for [28]Si taken from Ref. [14] and the calculated values is obtained by using the SkX parameterization. For this reason, the SkX parameterization is used to calculate the nuclear densities for all other Si-isotopes.

The values thus obtained for the charge densities of these isotopes at the center, r = 0, have decreased approximately from 0.08 fm[-3] for [28]Si to 0.057 fm[-3] for [40]Si with the increasing number of neutrons (see Fig. 3-a). The proton densities at the center are equal to the neutron densities because Z = 14, and N =14 for [28]Si, Fig. 3-b.
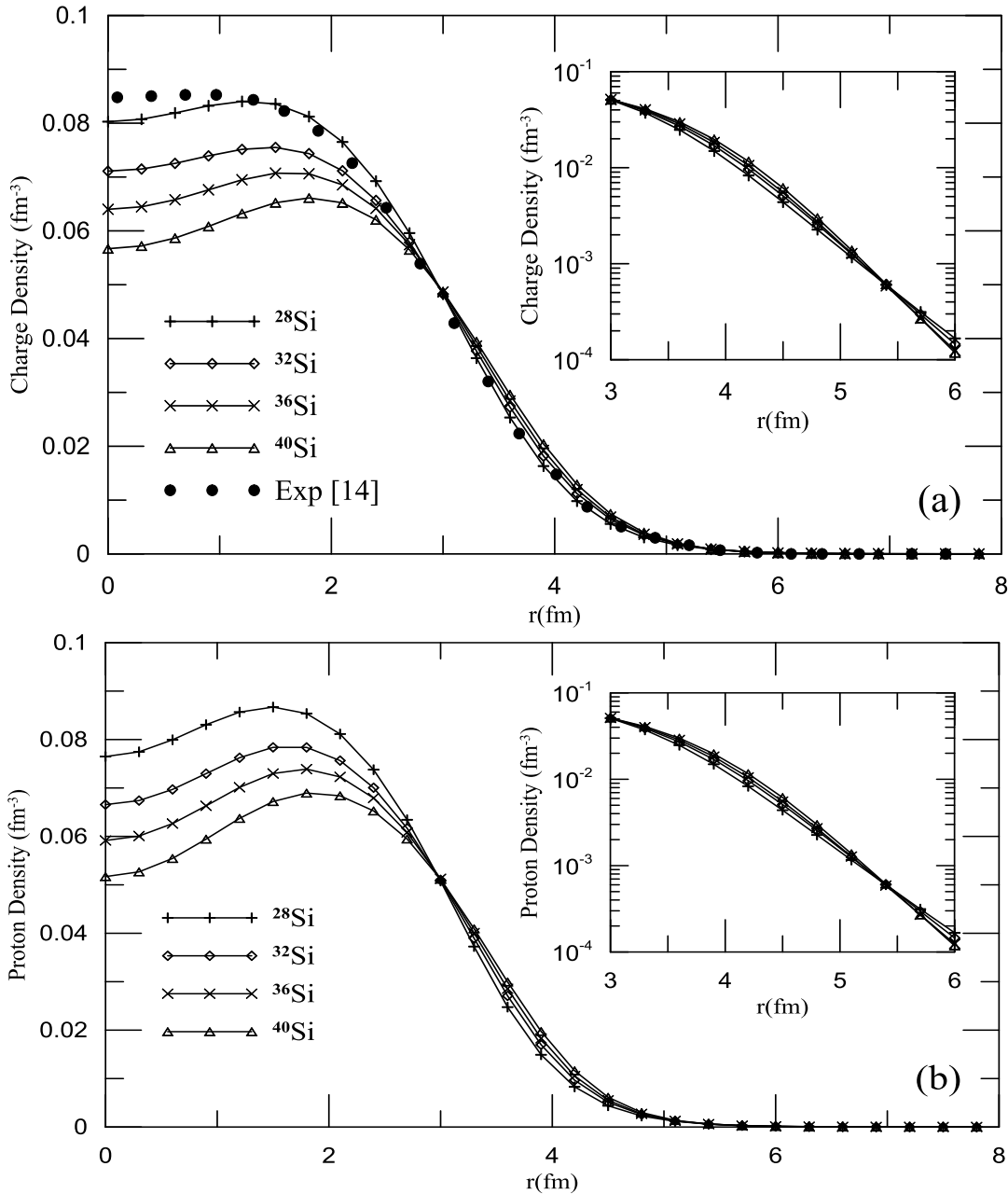

Fig.3: Density curves of different Si- isotopes calculated by the SkX parameterization; (a) charge density, (b) proton density.

As a general rule, it can be noted that with increasing number of neutrons and constant number of protons in the succeeding isotopes of one and the same element the neutron density increases whereas the proton density decreases accordingly. This rule applies to the range r > 1.4 fm, as to the range 0 ~ 1.4 fm. The rule stated above is violated and the abnormal behavior of the isotopes can be seen clearly in Fig. 4c. The mass density is also governed by the same rule which applies to the range r > 2 fm but is violated for the range

r ≤ 2 fm, Fig.4d. In this range the abnormality (randomness) in the behavior of the isotopes (i.e. oscillations in density values) is due to the diffusion of the nuclear matter in the vicinity of the center of the nucleus. This abnormal behavior results from the stretching of the density distribution as the isotopes increase progressively in mass number. Consequently, the applied Skyrme parameterization fails to give an exact description in the said region.
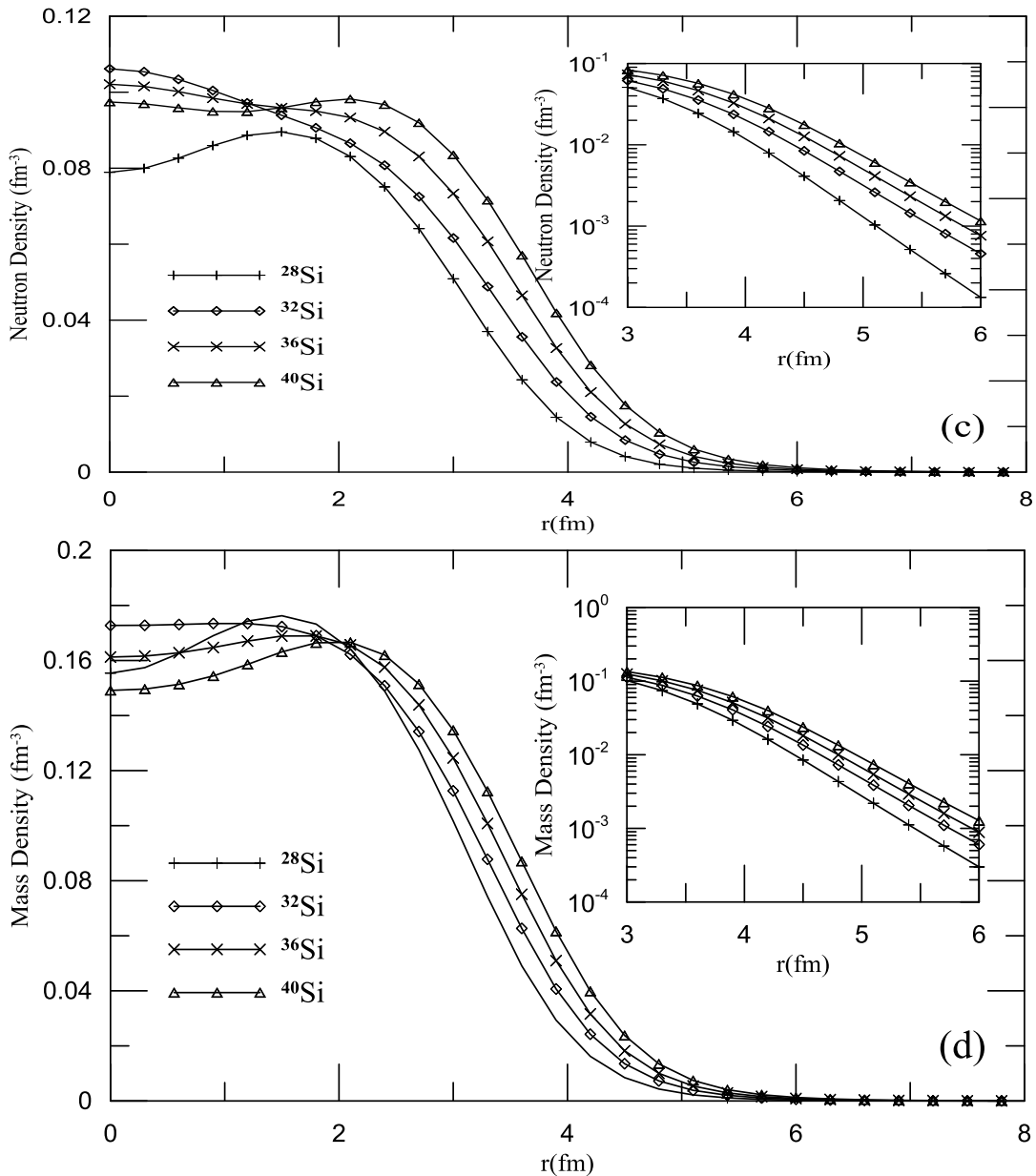
Fig. 4: Density curves of different Si- isotopes calculated by the SkX parameterization; (c) neutron density, (d) mass density.

For more illustration the calculated charge density distributions for Si-isotopes are displayed as a surface in Fig. 5. These distributions are plotted against the nuclear masses are decreasing (in viewing into the page). These variations of charge densities are best portrayed in block form.
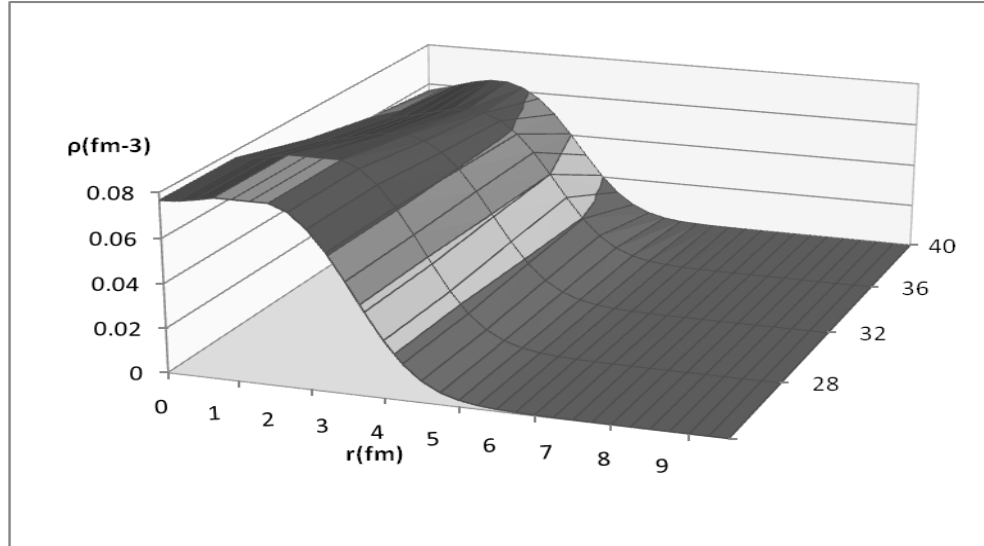

Fig. 5: Charge density variation with mass number from SkX parameterization for different Si- isotopes.

The charge probability density $P(r)_{ch}$ represents the probability to find Z protons at a given radius r from the center of the nucleus as given by Eq. (8). Although experimental data on charge probability density may not be available, it can, however, be easily calculated from the experimental data already available on nuclear charge density. The charge densities of the four isotopes are calculated by the Skyrme parameterizations that yielded the best agreement with the experimental data and these same parameterizations were then employed in calculating the probability densities. The calculated and experimental probability densities of the ^{28}Si turned out to be in good agreement and their curves show a clear shift forward (to the right) with increasing radii (also increasing mass numbers) of the elements as shown clearly in Fig. 6.
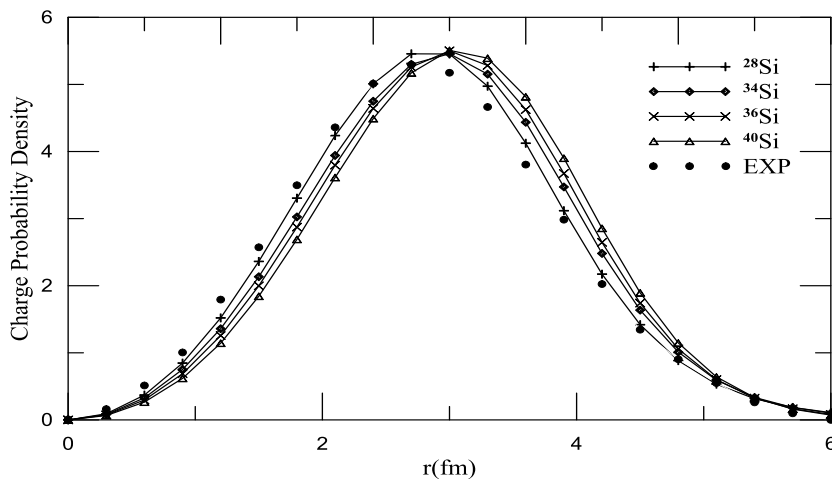

Fig. 6: Comparison of the experimental and theoretical charge probability density distributions for ^{28,32,36,40}Si, by using the SkX-parameterization.

The rms charge radius is a fundamental property of the atomic nucleus. The rms radii of charge distributions can be evaluated from the charge densities according to Eq.(9). It can be seen in Fig. 7 that the calculations by the SHF- method of the nuclear charge rms radii of the isotopes of the Si reveal a good conformity among the curves in each drawing separately and in the drawing combined. All the curves based on the different parameter sets considered in the drawing have more or less the same functional form, and are generally displaced vertically relative to each other with the SkM*- curve as the upper one and the S1-curve as the lower for all the isotopes.
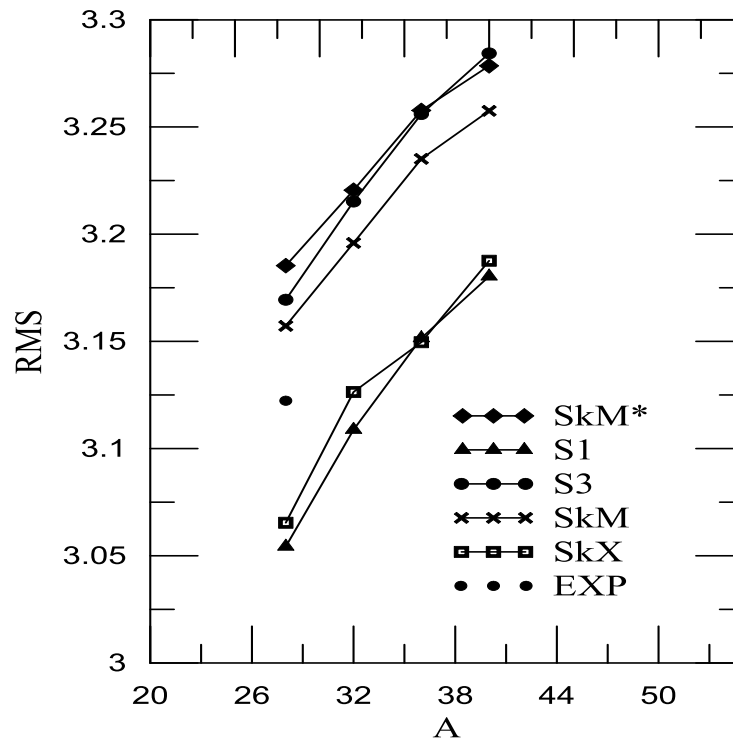

Fig. 7: The RMS- values of: Si-isotopes, for different Skyrme interaction parameters.

The rms charge radii for ^{28}Si and ^{40}Si decrease from (3.1853) and (3.2785) by SkM* to (3.0543) and (3.1803) by S1 as shown in Table 2.

Table 2: The calculated values of nuclear charge rms radii compared with experimental values taken from Ref. [17].

Nucleus	SkM*	S1	S3	SkM	SkX	Exp(rms)
28Si	3.1853	3.0543	3.1694	3.1572	3.0654	3.1223
32Si	3.2205	3.1088	3.2152	3.1959	3.1264	………..
36Si	3.2577	3.1515	3.2560	3.2351	3.1496	………..
40Si	3.2785	3.1803	3.2843	3.2575	3.1876	………..

Fig. 8 shows a comparison between the experimental and theoretical binding energies plotted against the mass number, A, for the Si-isotopes. The Skyrme parameterizations SkM*, S1, S3, SkM, and SkX are used in the calculations. Except for some slight deviations in the S1- curves all the other curves generally show the same behavior in the four drawing as shown below.
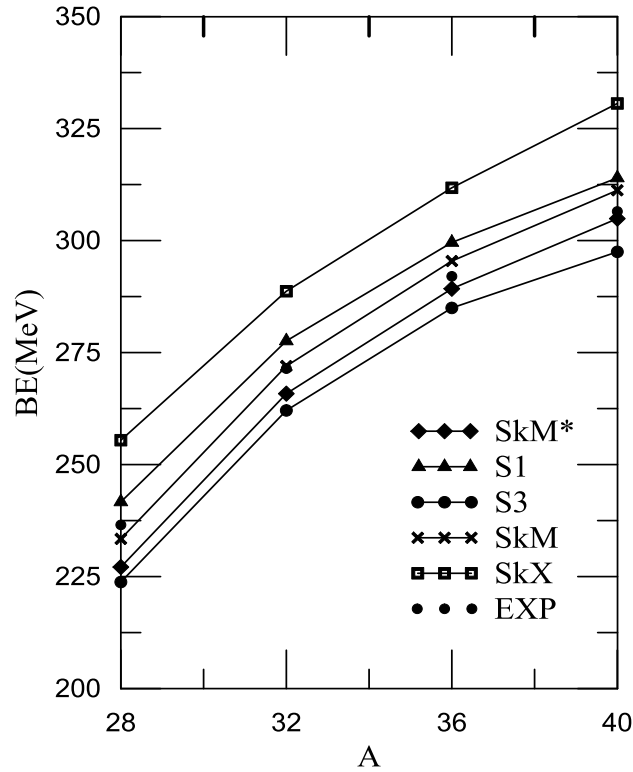
Fig. 8: The binding energy of: Si-isotopes, for different Skyrme interaction set parameters.

The SkM*- based binding energies have the highest values for all the isotopes of each of the four element whereas the S3- based values are the lowest. The SkM- based binding energy values turn out to be in full agreement with the experimental data as can be clearly seen in Table 3. For this reason we have selected the SkM parameterization as a basis for calculating the form factors of the selected nuclides.

Table 3: The calculated values of Binding energy compared with experimental values taken from Ref. [18].

Nucleus	SkM*	S1	S3	SkM	SkX	Exp(B.E)
28Si	227.13	241.67	223.78	233.41	255.44	236.5356
32Si	265.83	277.60	262.08	271.99	288.69	271.4112
36Si	289.25	299.58	284.96	295.43	311.78	292.014
40Si	304.90	313.98	297.48	311.22	330.60	306.496

The skin thickness of a nucleus is defined as the distance over which the charge density drops from 90% to 10% of its maximal value. The thickness is almost the same for all heavy nuclei and is given by: t = 2a ln 9 ~ 2.40 fm [19]. The growth of the neutron skin with increasing neutron number was calculated for several isotopes from nuclear and charge-size data [20]. The thickness of neutron skin can be deduced from the difference between the radii of neutron and proton distributions. The neutron skin thickness is generally given by the Eq.(10) which was employed in the present calculations. The skin thickness property of a nucleus is, however, a quantity which is rather difficult to observe experimentally. That is why the experimental value of this property is not so available in the literature and comparison is only with the theoretical values.

The neutron skin thickness of Si-isotopes increases with increasing mass number along

all the curves plotted by the different Skyrme parameterizations as shown in Fig.9.

In Table 4 the quantity t for some of the isotopes have negative values as a result of force tends to spread the protons a little, and

becomes increasingly positive with increasing neutron excess. These results are generally conformant with those obtained by Brack et al[21].
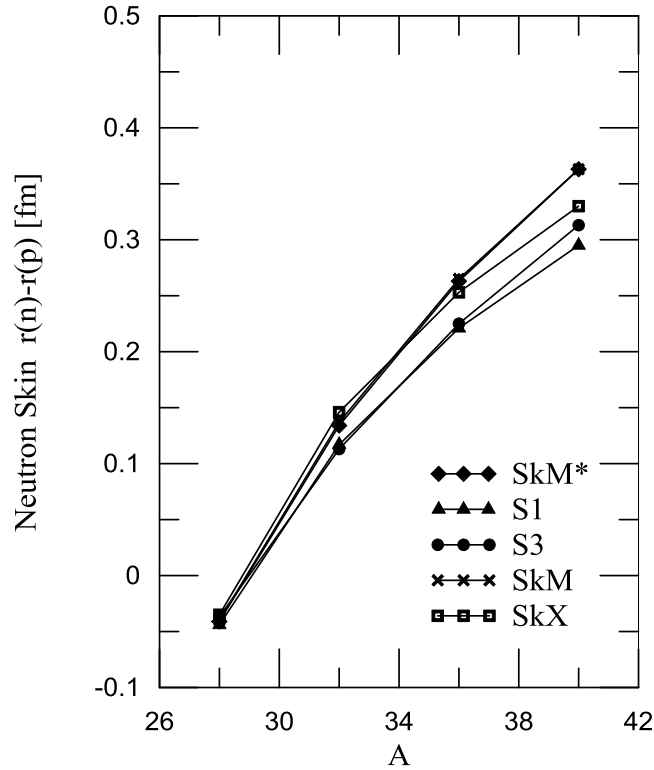

Fig. 9: The neutron skin of Si-isotopes, calculated by different Skyrme parameterizations.

Table 4: The skin thickness of the selected isotopes calculated by different Skyrme parameterizations.

Nucleus	SkM*	S1	S3	SkM	SkX
28Si	-0.041	-0.044	-0.037	-0.04	-0.035
32Si	0.134	0.117	0.113	0.137	0.146
36Si	0.263	0.221	0.225	0.265	0.253
40Si	0.363	0.295	0.313	0.363	0.33

From the charge densities shown in Fig. 3 the scattering amplitude form factors $|F(q)|^2$ are calculated for the isotopes of the selected element and shown in Fig. 10.

The experimental data (hollow circles) are given over the range of momentum transfers and compared with the theoretical values of the form factors calculated with SkX parameterization (since this set gives the best

agreement of the experimental data). The calculations will be discussed as follows;

The form factors calculated with SkX parameterization are in good agreement with the experimental data in the range of momentum transfer $q \leq 2.4$ fm^{-1} but they underestimate the experimental data for high q.
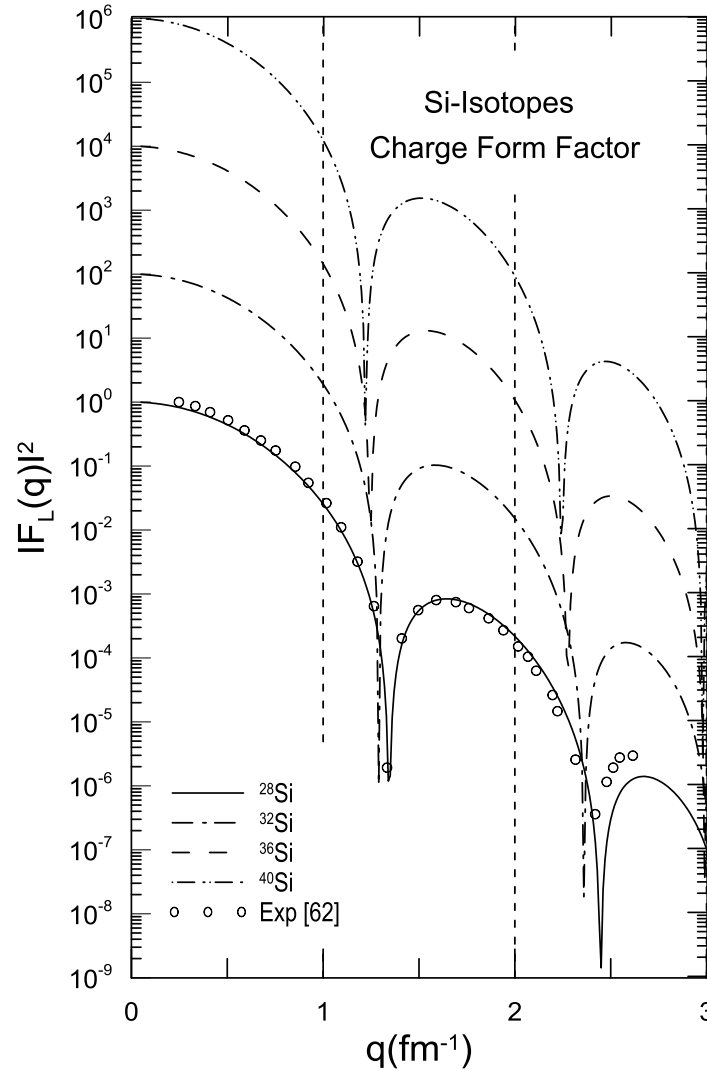
Fig.10: Longitudinal scattering form factors for ^{28}Si, ^{32}Si ($\times 10^2$), ^{36}Si ($\times 10^4$), ^{40}Si ($\times 10^6$). The experimental data are taken from Ref. [14].

This underestimation is ascribed to two factors. First, the Skyrme interaction approximation undergoes a low-momentum expansion, and the density fluctuation resulting from this approximation is expected to break down at some point. Second, mesonic-exchange corrections to the charge form factor become increasingly important at higher momentum transfers [21].

Conclusions

Calculations with SkX parameterization show the best agreement with the experimental data. However in the vicinity of the nucleus center (on the range r < 2 fm) the isotopes behave randomly with oscillating density values due to the diffusion (stretching) of the nuclear matter, which make Skyrme parameterizations fail to give an exact description in the said region. For the binding energy, the SkM parameterization also gives the best agreement between calculations and experimental data. Comparison between experiment and theory in terms of form factors has been discussed, where the data are taken over the range of momentum measured, and in terms of the charge densities. Rapid oscillations may occur in the experimental densities. Comparison with experiment will provide a test of the mean-field models.

References
[1] T. H. R. Skyrme, Phil. Mag. 1 (1956), 1043; Nucl. Phys., 9 (1959) 615.
[2] D. Vautherin and D. M. Brink, Phys. Rev., C5 (1972) 626.
[3] J. Friedrich, P. G. Reinhard, Phys. Rev., C33 (1986) 335.
[4] T.Skyrme, Nuclear Physics, 9(1959) 615.
[5] W.Greiner, J.Maruhn, "Nuclear Models" Second Edition, Berlin: Springer. 1996.
[6] L.G. Qiang, J. Phys., G 17 (1991) 134.
[7] J. Bartel, P. Quentin, M. Brack, C. Guet, and M.B. Hakansson, Nucl. Phys. A386 (1982) 79.
[8] L.X. Ge, Y.Z. Zhuo, W. Norenberg, Nucl. Phys. A 459 (1986) 77.
[9] B.A. Brown, Phys. Rev. C58 (1998) 220.
[10] B. Emma Suckling, Ph.D. Thesis, University of Surrey (2011).
[11] M. Bender, P. H. Heenen, P. G. Reinhard, Rev. Mod. Phys., 75 (2003) 121.
[12] B. Emma Suckling, MSc. Thesis, University of Surrey (2006).
[13] K. Langanke, J.A. Maruhn, S. E. Koonin, Computational Nuclear Physics 1, Springer-Verlag (1991).
[14] W. A. Richter, B. A. Brown, Phys. Rev., C67 (2003) 034317.
[15] M. Brack, C. Guet, H.-B. Haakansson, Phys. Lett. 123 (1985) 275.
[16] H. Uberall "Electron Scattering From Complex Nuclei (part A)" Academic Press-New York and London (1971).
[17] I. Angeli, Table of Nuclear Root Mean Square Charge Radii, INDC (HUN)-033(1999).
[18] Y.S. Shen, Z.Z. Ren, Phys. Rev., C54 (1996) 1158.
[19] C. Ian Brock, V Physik, Nuclear and Particle Physic (2012).
[20] A. Ozawa, T. Suzuki, I. Tanihata, Nucl. Phys. A693 (2001) 32.
[21] M. Brack, C.Guet, H.B.Hakansson, Phys. Rep. 123 (1985) 275-36.